Heliyon 10 (2024) e34763

Contents lists available at ScienceDirect

Heliyon

journal homepage: www.cell.com/heliyon

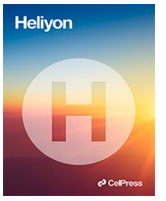

Research article

Relationship between pericoronary adipose tissue attenuation value and image reconstruction parameters

Lihong Chen [a,1], Le Cao [a,1], Bing Liu [a], Jianying Li [b], Tingting Qu [a], Yanshou Li [a], Yanan Li [a], Ning Pan [c], Yannan Cheng [a], Ganglian Fan [a], Zhijie Jian [a], Jianxin Guo [a,*]

[a] Department of Radiology, The First Affiliated Hospital of Xi'an Jiaotong University, #277 West Yanta Road, Xi'an, 710061, Shaanxi, China
[b] CT Imaging Research Center, GE Healthcare, #1 GuangHua Road, Chaoyang District, Beijing, 100010, China
[c] Bayer Healthcare Company Limited, #88 South Guanzheng Road, Xi'an, 710061, China

ARTICLE INFO

Keywords:
Computed tomography angiography
Coronary artery disease
Adipose tissue
Atherosclerosis
Reproducibility of results

ABSTRACT

Rationale and objectives: To investigate the relationship between the pericoronary adipose tissue CT mean attenuation ($PCAT_{MA}$) measurement and image reconstruction parameters (adaptive statistical iterative reconstruction-veo (ASIR-V) percentage, kernel, and slice thickness).
Materials and methods: One hundred and ninety-eight consecutive patients underwent CT coronary angiography at 100 kilovoltage peak (kVp) (n = 102) and 120 kVp (n = 96) were included. All scans were reconstructed by three means: 1. with 11 different ASIR-V percentages, standard kernel and 0.625 mm; 2. with soft, standard, detail, and bone kernels, 60 % ASIR-V, and 0.625 mm; 3. at 0.625 mm and 1.25 mm slice thickness, standard kernel and 60 % ASIR-V. $PCAT_{MA}$ of the three main coronary arteries was calculated using a dedicated software. Linear regression, analysis of variance (ANOVA), Friedman test, and paired *t*-test were used for statistical analysis.
Results: Linear regression of pooled average data showed that the $PCAT_{MA}$ was positively and linearly correlated with the ASIR-V percentage (all R squared >0.99). Regression analysis of individual data showed that most R squared were greater than 0.8 or 0.9, but their slope consisted of a relatively wide range. The difference of $PCAT_{MA}$ among different kernels for each coronary artery reached statistically significant levels ($P < 0.001$), particularly for the difference between standard and bone kernel. Most of the differences between 0.625 mm and 1.25 mm for LAD, LCX, and RCA at 100 kVp and 120 kVp reached statistical significance ($P < 0.001$).
Conclusions: $PCAT_{MA}$ correlates linearly with the strength of ASIR-V. Reconstruction kernel and slice thickness also affect $PCAT_{MA}$, especially for the sharp kernels.

1. Introduction

Coronary artery disease caused by atherosclerosis is a major cause of disability and death [1]. Studies have shown that

Abbreviations: ANOVA, Analysis of variance; **ASIR-V**, Adaptive statistical iterative reconstruction-veo; **CCTA**, Coronary computed tomography angiography; **HU**, Hounsfield unit; **kVp**, Kilovoltage peak; **LAD**, Left anterior descending; **LCX**, Left circumflex artery; **$PCAT_{MA}$**, Pericoronary adipose tissue CT mean attenuation; **RCA**, Right coronary artery; **SD**, Standard deviation; **VOI**, Volume of interest.

* Corresponding author.
E-mail address: gjx1665@xjtufh.edu.cn (J. Guo).

[1] These authors contributed equally to the work.

https://doi.org/10.1016/j.heliyon.2024.e34763
Received 23 August 2023; Received in revised form 15 July 2024; Accepted 16 July 2024
Available online 16 July 2024

inflammation plays a key role in the mechanism of atherosclerotic plaque formation and rupture [2,3]. The pericoronary adipose has an intimate anatomical and functional relationship with the coronary vasculature and regulates the coronary vascular system through the secretion of multiple bioactives including adipocytokines, microvesicles and gaseous messengers [4,5]. At the same time, the function and secretion of pericoronary adipose are regulated by complex homeostatic mechanisms and local intercellular interactions [6]. Local inflammation can lead to a shift in pericoronary adipose tissue secretion from anti-inflammatory to pro-inflammatory [7,8], resulting in a decrease of the local intracellular lipid accumulation, which is manifested as increased pericoronary adipose tissue CT mean attenuation ($PCAT_{MA}$) and can be monitored by routine coronary computed tomography angiography (CCTA) [9–11]. Data from clinical trials have shown that the perivascular $PCAT_{MA}$ can be used to improve cardiac risk prediction and stratification beyond the current state of-the-art assessment in CCTA [12–14]. Since the $PCAT_{MA}$ is defined as the average CT attenuation of adipose tissue (voxels with CT attenuation within a predefined window (−190 to −30 HU)) within a volume of interest (VOI) [12], technical factors that affect the CT attenuation may also have an effect on the $PCAT_{MA}$, such as scanning tube voltage, reconstruction kernel, denoising algorithm and slice thickness. For the clinical application of $PCAT_{MA}$ for risk stratification or evaluation of therapeutic efficacy, the exact impact of these technical factors should be fully investigated. However, although there have been a few studies on the effect of scanning tube voltage and the virtual monoenergetic energy level [15,16], no patient study has yet been published on the relationship between the $PCAT_{MA}$ and reconstruction parameters.

Therefore, this study aimed to evaluate the relationship between $PCAT_{MA}$ and image reconstruction parameters (including the strength of adaptive statistical iterative reconstruction-veo (ASIR-V), reconstruction kernel, and slice thickness) at two routine scanning tube voltages (100 kVp and 120 kVp).

2. Materials and methods

2.1. Study population

This was a retrospective study and was compliant with the Declaration of Helsinki. Institutional ethical review board approval of this study protocol and informed consent were waived because no patient-related diagnosis and treatment would be interfered with. One hundred and ninety-eight patients with confirmed or suspected coronary artery disease who underwent CCTA examination were included. The exclusion criteria were as follows: 1. CCTA examination with poor image quality due to motion or metal artifacts. 2. Patients with moderate to severe coronary artery stenosis (i.e., cross-sectional area stenosis that greater than 50 %) or obvious coronary artery calcium (coronary artery calcium score > 10) located in the analyzed VOI. 3. Patients with $PCAT_{MA}$ could not be fully generated by the analysis software.

2.2. CCTA scan and image reconstruction

A total of 198 patients were enrolled, including 112 in October 2022 for preliminary investigation and 86 in March 2024 for sample size expansion. All patients were scanned on a 256-row detector CT (Revolution CT, GE HealthCare): 102 at 100 kilovoltage peak (kVp)

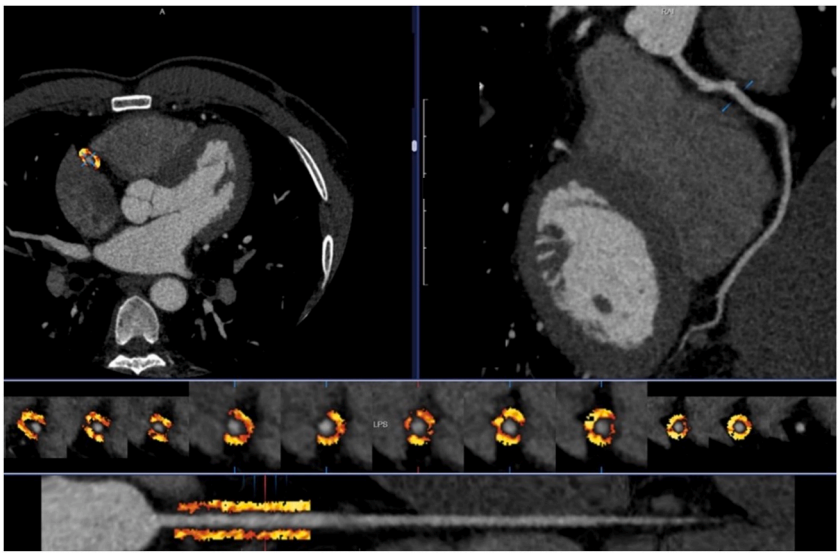

Fig. 1. A case example for $PCAT_{MA}$ analysis. The dedicated software (coronaryFAIdoc, Shukun technology, Shanghai, China) automatically segmented and labelled the anatomy of the heart and the coronary arteries. Then the volume of interests of LAD, LCX, and RCA were generated. Finally, the $PCAT_{MA}$ for LAD, LCX, and RCA was calculated according to the given threshold (−190 to −30 HU), respectively. $PCAT_{MA}$: pericoronary adipose tissue mean attenuation. LAD: left anterior descending artery; LCX: left circumflex artery; RCA: right coronary artery.

and 96 at 120 kVp, with a constant noise index of 21 Hounsfield unit (HU) and automatic tube current adjustment. 40–50 ml of iopromide 370 (Ultravist, Bayer AG) was administrated intravenously by a power injector at a flow rate of 4–5 ml/s, followed by 40 ml of saline at the same flow rate. Both the exact volume and flow rate were at the discretion of the radiographers, based on their experience and the patient's weight. CCTA image reconstruction parameters were as follows: 1. with 11 different ASIR-V percentages (0 %–100 % in 10 % step) with standard kernel and 0.625 mm thickness to investigate the effect of iterative reconstruction strength on $PCAT_{MA}$; 2. with soft, standard, detail, and bone kernels at a constant ASIR-V percentage of 60 % and 0.625 mm slice thickness to investigate the effect of reconstruction kernels; 3. at image slice thicknesses of 0.625 mm and 1.25 mm with the standard kernel and a constant ASIR-V percentage of 60 % to investigate the effect of slice thickness.

2.3. $PCAT_{MA}$ analysis

Post-processing of CCTA images and calculation of $PCAT_{MA}$ were performed using a dedicated artificial intelligence-based software (CoronaryFAIdoc version 1.1, Shukun technology, Shanghai, China), which automatically segments and labels the anatomy of the heart and the coronary arteries. As described in other previous studies [12], the proximal 40 mm of the left anterior descending artery (LAD), the left circumflex artery (LCX), and the proximal 10–50 mm of the right coronary artery (RCA) were automatically traced to extract the VOI, which was defined as a concentric circle extending radially 4 mm from the outer vessel wall. Compared with previous studies [12], we used a constant extending distance (4 mm) from the outer vessel wall instead of the mean diameter of the coronary artery due to the limitations of the post-processing software, which only allowed us to use an integral extending distance from 1 mm to 8 mm. Every VOI was checked by an experienced cardiothoracic radiologist (with 15 years of experience) to ensure that no coronary artery lumen or other high-attenuation tissue belonging elsewhere was included. The software then automatically calculated the $PCAT_{MA}$ of the VOI by averaging the attenuation of voxels within the target threshold of −190 to −30 HU for LAD, LCX, and RCA (Fig. 1).

2.4. Statistical methods

Normality tests for continuous variables were performed using the Shapiro-Wilk test. Normally distributed and non-normally distributed continuous variables were presented as mean ± standard deviation (SD) and median (1st, 3rd quartile), respectively. Analysis of variance (ANOVA) or Friedman test was used to compare the difference between the standard kernel and other kernels, followed by multiple comparison test with Dunnett's correction. Paired *t*-test and Wilcoxon rank sum test were used to compare the difference between 0.625 mm and 1.25 mm slice thickness, depending on the normality of the $PCAT_{MA}$ data. Linear regression was used to analyze the relationship between $PCAT_{MA}$ and the percentage of ASIR-V at the coronary artery level for each patient and their

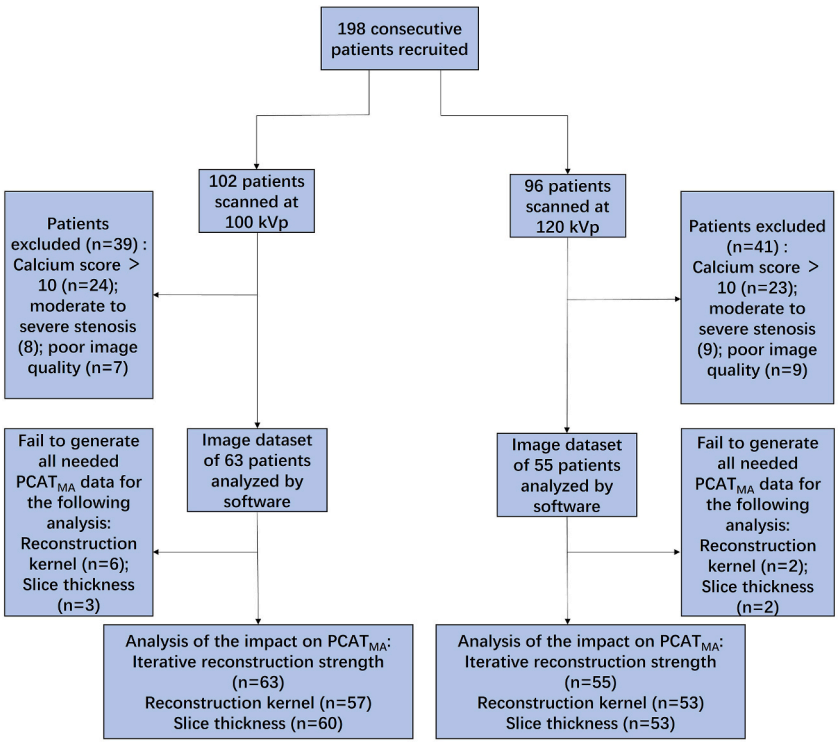

Fig. 2. Flowchart of patient inclusion and $PCAT_{MA}$ analysis. $PCAT_{MA}$: pericoronary adipose tissue mean attenuation.

pooled average $PCAT_{MA}$.

3. Results

3.1. Study population

Among the one hundred and ninety-eight consecutive patients, thirty-nine of the patients scanned at 100 kVp and forty-one of the patients scanned at 120 kVp were excluded due to significant coronary calcium, or moderate to severe coronary artery stenosis, or motion artifacts. The image dataset of the remaining patients was included in the subsequent $PCAT_{MA}$ analysis, and several patients were further excluded in the analysis of the effect of reconstruction kernel (6 scanned at 100 kVp; 2 scanned at 120 kVp) or slice thickness (3 scanned at 100 kVp; 2 scanned at 120 kVp) because the analysis software was unable to generate all the required $PCAT_{MA}$ data for them. The flowchart of patient inclusion and $PCAT_{MA}$ analysis is shown in Fig. 2. The baseline characteristics of the included patients are summarized in Table 1.

3.2. Influence of iterative reconstruction strength on $PCAT_{MA}$

In this part, $PCAT_{MA}$ was all normally distributed for each coronary artery in each set of images reconstructed with different percentages of ASIR-V, regardless of the scan tube voltage. Linear regression for the pooled average $PCAT_{MA}$ showed that the R squared for RAD, LCX, and RCA was 0.998, 0.999, and 0.996 at 100 kVp, and 0.995, 0.996, and 0.992 at 120 kVp, respectively, indicating that as the iterative reconstruction strength increased from 0 % to 100 %, the corresponding $PCAT_{MA}$ increased linearly, regardless of whether patients were scanned with 100 or 120 kVp tube voltage (Fig. 3a–f). The slope for LAD, LCX, and RCA was 0.078, 0.094, and 0.073 at 100 kVp, and 0.083, 0.099, and 0.084 at 120 kVp, respectively, showing an increase in $PCAT_{MA}$ of approximately 7–10 HU as the iterative reconstruction strength increased from 0 to 100 %, as shown in Fig. 3.

Linear regression for individual $PCAT_{MA}$ showed that the median (1st, 3rd quartile) R squared of LAD, LCX, and RCA was 0.98 (0.97, 0.99), 0.98 (0.97, 0.99), and 0.96 (0.91, 0.99) at 100 kVp, and 0.98 (0.97, 0.98), 0.98 (0.97, 0.99), and 0.97 (0.94, 0.98) at 120 kVp, respectively. A large proportion of these R squared were greater than 0.8 and 0.9, especially for those of LAD and LCX, as shown in Table 2 and Fig. 4. The range of regression slope for LAD, LCX, and RCA was 0.026–0.13, 0.035–0.16, and −0.027∼0.16 at 100 kVp, and 0.045–0.15, 0.055–0.22, and 0.020–0.20 at 120 kVp, respectively, as shown in Table 2 and Fig. 5.

3.3. Influence of the reconstruction kernel on $PCAT_{MA}$

In this part, only one data set was non-normally distributed: the $PCAT_{MA}$ of the RCA in the bone kernel reconstructed images of patients scanned at 100 kVp. Except that, the $PCAT_{MA}$ data of each coronary artery were all normally distributed, regardless of the reconstruction kernel and tube voltage used. The $PCAT_{MA}$ of LAD, LCX, and RCA for patients scanned at 100 kVp or 120 kVp and reconstructed with different kernels are shown in Table 3. ANOVA or Friedman test showed that there was a significant difference among the $PCAT_{MA}$ for different reconstruction kernels ($P < 0.001$). Subsequent multiple comparisons showed that the mean $PCAT_{MA}$ of all coronary arteries from bone kernel reconstructed images were all significantly lower than those from standard kernel reconstructed images, regardless of the scan tube voltage. The mean differences of $PCAT_{MA}$ (between standard kernel and the other three kernels) for soft and detail kernel were smaller than those for bone kernel. In some cases, including LAD, LCX, and RCA in images reconstructed with soft kernel at 100 kVp, RCA in images reconstructed with detail kernel at 100 kVp, and LCX in images reconstructed with soft and detail kernel at 120 kVp, the difference still reached statistical significance, as shown in Table 3.

3.4. Influence of the slice thickness on $PCAT_{MA}$

The $PCAT_{MA}$ data for LAD, LCX, and RCA for both 0.625 mm and 1.25 mm slice thickness were all normally distributed regardless of the scan tube voltage. Therefore, paired *t*-test was used for comparison. The $PCAT_{MA}$ of LAD, LCX, and RCA for different slice

Table 1
Baseline characteristics of the patients included in statistical analysis.

Scanning tube voltage	100 kVp	120 kVp
Patients (n)	63[a]	55[b]
Male sex (%)	34 (54 %)	31 (56 %)
Age (year)	51.2 ± 15.7	54.9 ± 10.1
body mass index (kg/m2)	24.5 ± 3.5	23.5 ± 6.9
Clinical symptoms		
Typical angina pectoris (%)	5(8 %)	4 (7 %)
Atypical chest pain (%)	42 (67 %)	33 (60 %)
Dyspnoea (%)	16(25 %)	18 (33 %)

[a] : 6 and 3 of them were excluded in the analysis of the effect of reconstruction kernel and slice thickness, respectively.
[b] :2 of them was excluded in the analysis of the effect of reconstruction kernel and slice thickness.

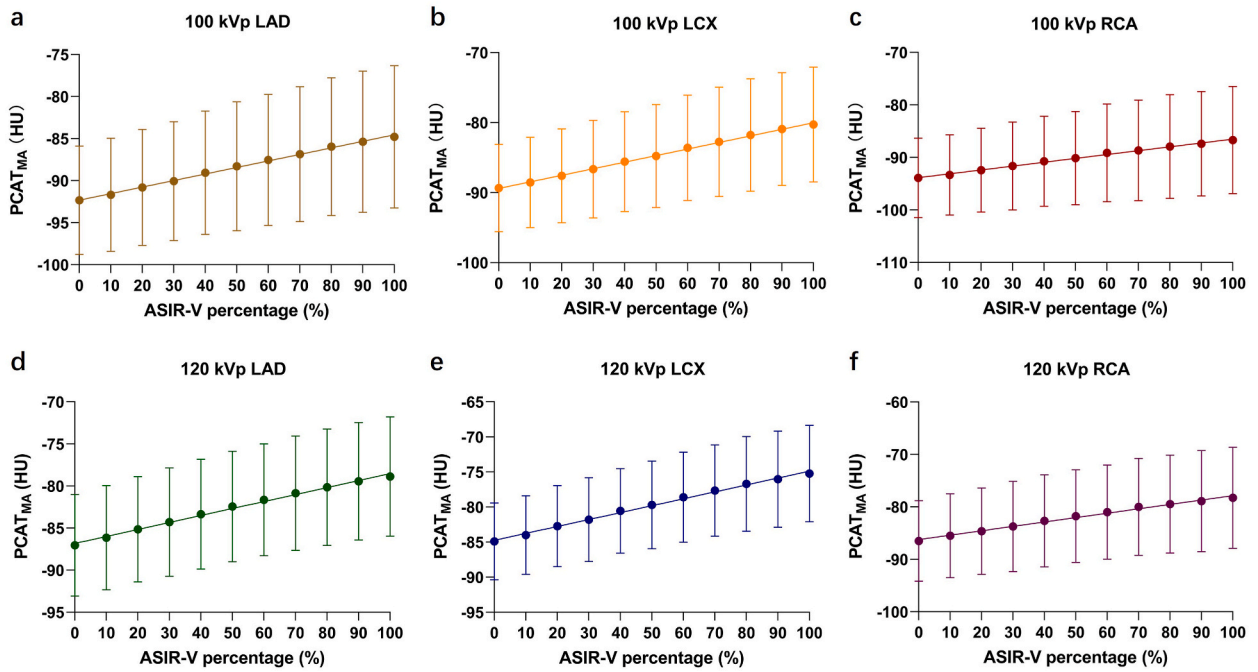

Fig. 3. Positive and Linear correlation between the pooled average $PCAT_{MA}$ and the percentage of ASIR-V for LAD, LCX, and RCA at 100 kVp and 120 kVp. Panel a, b, and c show the average $PCAT_{MA}$ for LAD, LCX, and RCA at 100 kVp, respectively, while panel d, e, and f show the average $PCAT_{MA}$ for LAD, LCX, and RCA at 120 kVp, respectively. LAD: left anterior descending artery; LCX: left circumflex artery; RCA: right coronary artery. $PCAT_{MA}$: pericoronary adipose tissue mean attenuation.

Table 2
The slope and R squared of linear regression for individual $PCAT_{MA}$.

Tube voltage	Coronary arteries	Slope		R Squared			
		Range	Mean ± SD	Range	median (1st, 3rd quartile)	> 0.9	> 0.8
100 kVp (n = 63)	LAD	0.026–0.13	0.077 ± 0.027	0.80–1.0	0.98 (0.97, 0.99)	59 (93.6)	63 (100 %)
	LCX	0.035–0.16	0.093 ± 0.028	0.84–1.0	0.98 (0.97, 0.99)	62 (98.4 %)	63 (100 %)
	RCA	−0.027~0.16	0.073 ± 0.036	0.05–0.99	0.96 (0.91, 0.99)	48 (76.2 %)	52 (82.5 %)
120 kVp (n = 55)	LAD	0.045–0.15	0.083 ± 0.020	0.89–1.0	0.98 (0.97, 0.98)	54 (98.2 %)	55 (100 %)
	LCX	0.055–0.22	0.099 ± 0.028	0.93–1.0	0.98 (0.97, 0.99)	55 (100 %)	55 (100 %)
	RCA	0.020–0.20	0.084 ± 0.029	0.27–1.0	0.97 (0.94, 0.98)	45 (81.8 %)	51 (87.1 %)

$PCAT_{MA}$: pericoronary adipose tissue mean attenuation; LAD: left anterior descending artery; LCX: left circumflex artery; RCA: right coronary artery.

thicknesses at 100 kVp and 120 kVp are shown in Table 4. The mean difference (95 % CI) between 0.625 mm and 1.25 mm for LAD, LCX, and RCA was 1.38 (0.91–1.85), 1.43 (−0.91–1.65), and −0.53 (−0.16–1.2) at 100 kVp, and 1.19 (0.82–1.56), 1.79 (1.29–2.29), and 1.0 (−0.58–1.57) at 120 kVp. Although most of the absolute differences were less than or equal to 3 HU, most of the difference between 0.625 mm and 1.25 mm for LAD, LCX, and RCA at 100 kVp and 120 kVp reached statistical significance.

4. Discussion

Our study investigated the relationship between $PCAT_{MA}$ and image reconstruction parameters (including the strength of ASIR-V, reconstruction kernel, and slice thickness) at two routine scanning tube voltages. To the best of our knowledge, this is the first human study comprehensively investigating the relationship between the $PCAT_{MA}$ and the primary CT reconstruction parameters. The main findings of our study were as follows: (1) The $PCAT_{MA}$ increased linearly and significantly with increasing strength of ASIR-V. The linear regression equations were obtained for each coronary artery at both 100 kVp and 120 kVp. (2) Reconstruction kernels had a significant impact on the $PCAT_{MA}$, especially when a sharper kernel was used. (3) Slice thickness had a relatively small effect on the $PCAT_{MA}$, but the effect still reached statistical significance in most cases. Our study provided insights into the influence of image reconstruction parameters on $PCAT_{MA}$ and may therefore enable bias correction in $PCAT_{MA}$-related clinical practice and prediction model research.

Although several studies have reported the value of $PCAT_{MA}$ in differentiating the inflammatory status of coronary arteries and its usefulness in improving cardiac risk prediction [12–14], there are currently no major guidelines recommending the use of $PCAT_{MA}$ for

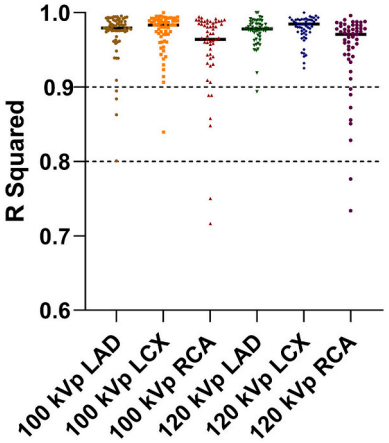

Fig. 4. The R squared of linear regression for individual $PACT_{MA}$ data. 5 data points in the 100 kVp RCA column and 2 data points in the 120 kVp RCA column exceeded the limitation of axis. LAD: left anterior descending artery; LCX: left circumflex artery; RCA: right coronary artery. $PCAT_{MA}$: pericoronary adipose tissue mean attenuation.

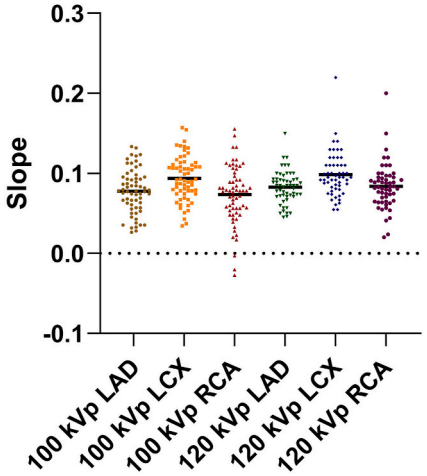

Fig. 5. The slope of linear regression for individual $PACT_{MA}$ data. LAD: left anterior descending artery; LCX: left circumflex artery; RCA: right coronary artery. $PCAT_{MA}$: pericoronary adipose tissue mean attenuation.

diagnosis or risk stratification, which may be due to the current situation of lack of high-quality evidence derived from rigorous randomized controlled clinical trials. For example, the European Society of Cardiology guidelines for the diagnosis and management of chronic coronary syndromes recommends the use of echocardiography, CCTA, or invasive coronary angiography to diagnose CAD or assess the risk of future cardiovascular events [17], in which the $PCAT_{MA}$ is not recommended. Ma et al. reported that the mean proximal $PCAT_{MA}$ of patients with and without coronary artery disease was −96.2 HU and −95.6 HU, respectively, and the lesion-specific $PCAT_{MA}$ of coronary artery with and without plaque was −94.7 HU and −97.2 HU, respectively, showing a small $PCAT_{MA}$ variation between coronary artery disease patients and healthy controls [18]. Similarly, the difference in $PCAT_{MA}$ was 5.0 HU between culprit and non-culprit lesions [19] and 5.6 HU between lesions with and without subsequent in-stent restenosis [20]. Goeller et al. reported that during a mean follow-up period of 3.4 years, the mean $PCAT_{MA}$ of the RCA increased by only 4.4 HU in patients with progressive non-calcific plaque burden [21]. These study results suggest that the variation of $PCAT_{MA}$ is small and easily submerged in the bias resulting from the inconsistency of technical parameters in the imaging chain [9,18–21]. To further improve the usefulness of $PCAT_{MA}$ in clinical practice and to well prepare a rigorous randomized controlled clinical trial, the effect of the technical factor in the imaging chain should be carefully investigated so that the bias from this chain can be corrected as much as possible, which justifies our study.

The strength of the iterative reconstruction tends to vary depending on the scanning task and institution. For example, it is determined by the clinical task and patient weight to achieve a balance between radiation dose and image noise [22,23]. In addition, the strength of the iterative reconstruction also depends on the acceptance of the “plastic-like” artifacts on the iterative reconstruction images, which varies considerably between image interpreters and between institutions in clinical practice. For example, regarding the best iterative reconstruction strength in CCTA, Dominik C et al. found that the ASIR-V 100 % provided the best image quality score

Table 3
The $PCAT_{MA}$ (HU) of LAD, LCX, and RCA for different reconstruction kernels at 100 kVp and 120 kVp.

Kernel		100 kVp (n = 57)			120 kVp (n = 53)		
		LAD	LCX	RCA[a]	LAD	LCX	RCA
Soft		−86.3 ± 7.7	−82.6 ± 7.5	−88.0 ± 9.4	−82.1 ± 7.8	−78.4 ± 6.2	−81.1 ± 9.0
Standard		−87.0 ± 7.3	−83.5 ± 7.3	−88.6 ± 9.2	−82.1 ± 5.8	−79.1 ± 5.7	−81.5 ± 8.3
Detail		−87.6 ± 7.2	−84.4 ± 7.2	−89.9 ± 8.7	−83.2 ± 6.38	−79.8 ± 5.8	−82.8 ± 8.4
Bone		−94.3 ± 5.3	−91.7 ± 5.2	−96.5 ± 6.2	−91.2 ± 5.9	−88.6 ± 5.4	−90.7 ± 7.4
ANOVA/ Friedman test	F	212	221	/	31	365	157
	P value	<0.001	<0.001	<0.001	<0.001	<0.001	<0.001
Standard vs Soft	Mean difference (95 % CI)	−0.72 (−0.94 ~ −0.5)	−0.91 (−1.2 ~ −0.64)	−0.63 (−0.98–0.36)	0 (−1.2–1.2)	−0.64 (−1.2 ~ −0.12)	−0.049 (−1.8–0.87)
	Rank sum difference	/	/	−36	/	/	/
	Adjusted P value	<0.001	<0.001	0.03	>0.999	0.012	0.713
Standard vs Detail	Mean difference (95 % CI)	0.53 (−0.24–1.3)	0.84 (−0.15–1.8)	1.3 (0.20–2.3)	1.1 (−0.06–2.2)	0.68 (0.11–1.3)	1.3 (−0.06–2.6)
	Rank sum difference	/	/	41	/	/	/
	Adjusted P value	0.244	0.064	0.009	0.66	0.016	0.064
Standard vs Bone	Mean difference (95 % CI)	7.3 (6.4–8.2)	8.2 (7.3–9.1)	7.9 (6.5–9.2)	9.0 (7.9–10)	9.5 (8.4–11)	9.2 (7.7–11)
	Rank sum difference	/	/	107	/	/	/
	Adjusted P value	<0.001	<0.001	<0.001	<0.001	<0.001	<0.001

$PCAT_{MA}$ value are presented as mean ± SD.
$PCAT_{MA}$: pericoronary adipose tissue mean attenuation; LAD: left anterior descending artery; LCX: left circumflex artery; RCA: right coronary artery.
[a] : Using Friedman test for analysis.

Table 4
The $PCAT_{MA}$ (HU) of LAD, LCX, and RCA for different slice thickness at 100 kVp and 120 kVp.

Tube voltage	Coronary arteries	slice thickness (mm)		Mean difference[a] (95%CI)	1st, 3rd quartile of difference	P value[a]
		0.625	1.25			
100 kVp (n = 60)	LAD	−87.2 ± 7.6	−85.9 ± 8.1	1.38 (0.91–1.85)	0,2	<0.001
	LCX	−83.4 ± 7.7	−82.0 ± 8.5	1.43 (−0.91–1.96)	1,2.75	<0.001
	RCA	−88.6 ± 9.1	−88.1 ± 9.7	−0.53 (−0.16–1.2)	0,2	0.126
120 kVp (n = 53)	LAD	−81.8 ± 6.7	−80.6 ± 7.1	1.19 (0.82–1.56)	1,2	<0.001
	LCX	−78.4 ± 6.5	−76.7 ± 7.2	1.79 (1.29–2.29)	1,3	<0.001
	RCA	−80.9 ± 8.8	−79.9 ± 9.1	1.08 (−0.58–1.57)	0,2	<0.001

$PCAT_{MA}$ value are presented as mean ± SD.
$PCAT_{MA}$: pericoronary adipose tissue mean attenuation; LAD: left anterior descending artery; LCX: left circumflex artery (LCX); RCA: right coronary artery (RCA).
[a] : The difference between $PCAT_{MA}$ for 0.625 mm and 1.25 mm slice thickness.

[24], but Pontone et al. found that ASIR-V 60 % provided the optimal balance between image noise, contrast-to-signal ratio, and image quality score [25]. The inevitable variations in the strength of the iterative reconstruction may introduce bias into the analysis of $PCAT_{MA}$ if the iterative reconstruction has a significant effect on it. Several studies have investigated the effect of iterative reconstruction on the attenuation of body tissues or simulated materials, and their results have been inconsistent. Protik et al. found that the addition of 50 % ASIR (the previous edition of ASIR-V) had no effect on the CT attenuation of 7 simulated materials [26]. However, another study comparing six iterative reconstruction algorithms found that the CT attenuation of the Catphan 600 phantom uniformity module decreased steadily as the percentage of ASIR increased from 10 % to 90 % [27]. A patient study showed that the attenuation of the aortic root remained stable as the percentage of ASIR-V increased from 0 % to 100 %, while the attenuation of the left main artery and right coronary artery decreased linearly and significantly, suggesting that the effect of iterative reconstruction also varies in different body parts [28].

Regarding the effect of iterative reconstruction on pericoronary adipose tissue, to the best of our knowledge, only one study has investigated the difference between filtered back projection and iterative reconstruction using ex vivo porcine heart phantoms and showed that iterative reconstruction generated a higher attenuation than FBP (the differences were about 12∼13 HU at 100 kVp and 13–18 HU at 120 kVp) [29], indicating that the use of iterative reconstruction significantly influenced $PCAT_{MA}$. However, this study had several limitations. Firstly, it did not reveal the strength of the iterative reconstruction used; secondly, it did not investigate the effect of different strengths of iterative reconstruction; thirdly, it was conducted with ex vivo porcine heart phantoms, so that the conclusions may not be applicable to humans. Our patient study investigated the relationship between $PCAT_{MA}$ and the strength of the ASIR-V for all three coronary arteries at routine scan voltages. We found that the pooled average $PCAT_{MA}$ increased linearly and

significantly with increasing strength of the iterative reconstruction, and the difference of $PCAT_{MA}$ between the lowest and highest strength of iterative reconstruction was about 7∼9 HU at 100 kVp and 8–10 HU at 120 kVp, which was partially consistent with the previous phantom studies [29], indicating that not only the use of iterative reconstruction, but also its strength significantly affected the $PCAT_{MA}$. We speculated that this positive correlation was due to the smoothing effect of iterative reconstruction, which improved the image uniformity and reduced the texture contrast in the coronary artery region. The linear regression equations for each coronary artery obtained in this study may be helpful to improve the comparability of $PCAT_{MA}$ in clinical practice and to refine the $PCAT_{MA}$-related cardiovascular outcome prediction model in academic research by allowing bias correction for different strengths of iterative reconstruction. However, although the regression analysis of individual data showed that the vast majority of the $PACT_{MA}$ was linearly correlated with the iterative reconstruction strength (most R squared were greater than 0.8), the slope of individual regression equations varied over a relatively wide range, indicating that the linear regression equations obtained in the pooled average $PCAT_{MA}$ analysis should be used prudently. To improve the effectiveness of bias correction for different strengths of iterative reconstruction, future studies exploring the personalized slope determination model with larger samples are warranted.

The effect of the reconstruction kernel on the CT attenuation of different coronary artery-related regions appeared to be variable according to a previous study by Cademartiri et al. [30]. They showed that the CT attenuation of non-calcified plaques in ex vivo coronary arteries decreased steadily with increasing reconstruction kernel sharpness, which was consistent with the results of another in-vivo patient study by Achenbach et al. [31]. However, the relationship between CT attenuation and kernel for the lumen, surrounding tissue, and calcified plaque appeared to be much different and complex [30]. Regarding $PCAT_{MA}$, to the best of our knowledge, there has been no study on the effect of reconstruction kernel on $PCAT_{MA}$. Our study showed that the reconstruction kernels had a significant effect on $PCAT_{MA}$, especially when a much sharper (bone) kernel was used. The mean differences between the standard kernel and the bone kernel for each coronary artery were much greater than those between the standard kernel and the soft kernel or the detail kernel at both 100 kVp and 120 kVp. These results were consistent with previous studies showing that the CT value of non-calcified plaque decreased much more when the sharpest kernel was used [31]. The effect of a bone kernel at a particular scanning tube voltage appeared to be similar, specifically, the mean difference for each coronary artery was approximately 7∼8 HU at 100 kVp and 9–10 HU at 120 kVp. This result may enable bias correction of $PCAT_{MA}$ when the bone kernel is used for patients with coronary stents. Fortunately, the mean difference between the standard kernel and the soft kernel, as well as the detail kernel, was relatively small, and half of the differences did not reach a statistical significance. This finding indicated that the changes between these three most commonly used kernels may only have a small impact on the clinical use of the $PCAT_{MA}$ index. However, since the difference in some circumstances still reached statistically significant and the variation of $PCAT_{MA}$ during disease progression is small [9,18–21], it is better to keep the same reconstruction kernel as in the previous CT for a follow-up $PCAT_{MA}$ imaging.

Although a thin slice thickness (usually <1 mm) is preferred in clinical practice to improve spatial resolution of the CCTA images, thicker slice thickness should still be considered for obese patients to reduce image noise [32]. To the best of our knowledge, no study has investigated the influence of slice thickness on the $PCAT_{MA}$. Our study showed that the difference in $PCAT_{MA}$ between 0.625 mm and 1.25 mm reached statistical significance in most cases, indicating that slice thickness had significant effect on $PCAT_{MA}$ for all three coronary arteries. Since the variation of $PCAT_{MA}$ during disease progression is small [9,18–21], it is also better to keep the same slice thickness as in the previous CT for a follow-up $PCAT_{MA}$ imaging to avoid bias.

Our study has several limitations. (1) Although the principle of the iterative reconstruction algorithms is similar for different vendors [33], the conclusions of this study may not be applicable to other vendor-specific iterative reconstruction algorithms. (2) A constant extending distance (4 mm) from the outer vessel wall was used to generate the VOI in this study instead of the mean diameter of the coronary artery as in previous studies. However, a cross-sectional survey showed that the diameter of the proximal coronary artery is close to 4 mm [34], and we believe that the conclusions of our study are generalizable when the mean diameter is used to generate the VOI. (3) The sample size of our study was relatively small. However, the linear correlation between $PCAT_{MA}$ and the strength of the iterative reconstruction, as well as the significant influence of the reconstruction kernel and slice thickness, were clearly demonstrated. These findings may not change significantly with a larger sample size.

In conclusion, the $PCAT_{MA}$ of coronary arteries correlates linearly with the strength of ASIR-V. Reconstruction kernel and slice thickness also affect the $PCAT_{MA}$, especially for the sharp kernel. $PCAT_{MA}$ values need to be interpreted in the context of the image reconstruction parameters.

Data availability statement

The data that support the findings of this study are available on request from the corresponding author.

Ethics approval and consent to participate

Ethical approval of this study protocol and informed consent were waived because of the retrospective nature of the study and the absence of intervention.

CRediT authorship contribution statement

Lihong Chen: Writing – original draft, Methodology, Investigation, Conceptualization. **Le Cao:** Writing – original draft, Investigation, Data curation. **Bing Liu:** Writing – original draft, Data curation. **Jianying Li:** Writing – review & editing. **Tingting Qu:** Writing – original draft. **Yanshou Li:** Data curation. **Yanan Li:** Writing – original draft. **Ning Pan:** Writing – review & editing. **Yannan Cheng:**

Writing – review & editing. **Ganglian Fan:** Writing – review & editing. **Zhijie Jian:** Writing – review & editing. **Jianxin Guo:** Supervision, Project administration.

Declaration of competing interest

The authors declare that they have no known competing financial interests or personal relationships that could have appeared to influence the work reported in this paper.

References

[1] Gregg W. Stone, et al., A prospective natural-history study of coronary atherosclerosis, N. Engl. J. Med. 364 (3) (2011) 226–235.
[2] Russell Ross, Atherosclerosis—an inflammatory disease, N. Engl. J. Med. 340 (2) (1999) 115–126.
[3] Peter Libby, Paul M. Ridker, Attilio Maseri, Inflammation and atherosclerosis, Circulation 105 (9) (2002) 1135–1143.
[4] Michał Konwerski, et al., Atherosclerosis pathways are activated in pericoronary adipose tissue of patients with coronary artery disease, J. Inflamm. Res. 14 (2021) 5419.
[5] Tomasz Mazurek, et al., Human epicardial adipose tissue is a source of inflammatory mediators, Circulation 108 (20) (2003) 2460–2466.
[6] Yasuhiro Onogi, et al., PDGFRβ regulates adipose tissue expansion and glucose metabolism via vascular remodeling in diet-induced obesity, Diabetes 66 (4) (2017) 1008–1021.
[7] Charles Caër, et al., Immune cell-derived cytokines contribute to obesity-related inflammation, fibrogenesis and metabolic deregulation in human adipose tissue, Sci. Rep. 7 (1) (2017) 1–11.
[8] Carey N. Lumeng, Jennifer L. Bodzin, Alan R. Saltiel, Obesity induces a phenotypic switch in adipose tissue macrophage polarization, J. Clin. Invest. 117 (1) (2007) 175–184.
[9] Alexios S. Antonopoulos, et al., Detecting human coronary inflammation by imaging perivascular fat, Sci. Transl. Med. 9.398 (2017) eaal2658.
[10] Jurrien H. Kuneman, et al., Pericoronary adipose tissue attenuation in patients with acute coronary syndrome versus stable coronary artery disease, Circulation: Cardiovascular Imaging (2023) e014672.
[11] Mohamed Marwan, et al., CT attenuation of pericoronary adipose tissue in normal versus atherosclerotic coronary segments as defined by intravascular ultrasound, J. Comput. Assist. Tomogr. 41 (5) (2017) 762–767.
[12] Evangelos K. Oikonomou, et al., Non-invasive detection of coronary inflammation using computed tomography and prediction of residual cardiovascular risk (the CRISP CT study): a post-hoc analysis of prospective outcome data, Lancet 392 (10151) (2018) 929–939.
[13] Nicola Gaibazzi, et al., Coronary inflammation by computed tomography pericoronary fat attenuation in MINOCA and tako-tsubo syndrome, J. Am. Heart Assoc. 8 (17) (2019) e013235.
[14] Pepijn A. van Diemen, et al., Prognostic value of RCA pericoronary adipose tissue CT-attenuation beyond high-risk plaques, plaque volume, and ischemia, Cardiovascular Imaging 14 (8) (2021) 1598–1610.
[15] Runlei Ma, et al., Towards reference values of pericoronary adipose tissue attenuation: impact of coronary artery and tube voltage in coronary computed tomography angiography, Eur. Radiol. 30 (2020) 6838–6846.
[16] Victor Mergen, et al., Epicardial adipose tissue attenuation and fat attenuation index: phantom study and in vivo measurements with photon-counting detector CT, Am. J. Roentgenol. 218 (5) (2022) 822–829.
[17] Juhani Knuuti, et al., 2019 ESC Guidelines for the diagnosis and management of chronic coronary syndromes: the Task Force for the diagnosis and management of chronic coronary syndromes of the European Society of Cardiology (ESC), Eur. Heart J. 41 (3) (2020) 407–477.
[18] R. Ma, M. Van Assen, D. Ties, et al., Focal pericoronary adipose tissue attenuation is related to plaque presence, plaque type, and stenosis severity in coronary CTA[J), Eur. Radiol. 31 (2021) 7251–7261.
[19] J.H. Kuneman, S.E. van Rosendael, P. van der Bijl, et al., Pericoronary adipose tissue attenuation in patients with acute coronary syndrome versus stable coronary artery disease, Circulation: Cardiovascular Imaging 16 (2) (2023) e014672.
[20] Z.F. Lu, W.H. Yin, U.J. Schoepf, et al., Prediction value of pericoronary fat attenuation index for coronary in-stent restenosis, Eur. Radiol. (2024) 1–10.
[21] M. Goeller, B.K. Tamarappoo, A.C. Kwan, et al., Relationship between changes in pericoronary adipose tissue attenuation and coronary plaque burden quantified from coronary computed tomography angiography[J), European Heart Journal-Cardiovascular Imaging 20 (6) (2019) 636–643.
[22] Seung Ho Kim, et al., Low-dose CT for patients with clinically suspected acute appendicitis: optimal strength of sinogram affirmed iterative reconstruction for image quality and diagnostic performance, Acta Radiol. 56 (8) (2015) 899–907.
[23] Bibi Martens, et al., Finding the optimal tube current and iterative reconstruction strength in liver imaging; two needles in one haystack, PLoS One 17 (4) (2022) e0266194.
[24] Dominik C. Benz, et al., Adaptive statistical iterative reconstruction-V: impact on image quality in ultralow-dose coronary computed tomography angiography, J. Comput. Assist. Tomogr. 40 (6) (2016) 958–963.
[25] Gianluca Pontone, et al., Impact of a new adaptive statistical iterative reconstruction (ASIR)-V algorithm on image quality in coronary computed tomography angiography, Acad. Radiol. 25 (10) (2018) 1305–1313.
[26] Angjelina Protik, et al., Phantom Study of the Impact of Adaptive Statistical Iterative Reconstruction (ASiR TM) on Image Quality for Paediatric Computed Tomography, 2012.
[27] Askell Löve, et al., Six iterative reconstruction algorithms in brain CT: a phantom study on image quality at different radiation dose levels, Br. J. Radiol. 86 (1031) (2013) 20130388.
[28] Dominik C. Benz, et al., Adaptive statistical iterative reconstruction-V: impact on image quality in ultralow-dose coronary computed tomography angiography, J. Comput. Assist. Tomogr. 40 (6) (2016) 958–963.
[29] Dominik Etter, et al., Towards universal comparability of pericoronary adipose tissue attenuation: a coronary computed tomography angiography phantom study, Eur. Radiol. (2022) 1–7.
[30] Filippo Cademartiri, et al., Influence of convolution filtering on coronary plaque attenuation values: observations in an ex vivo model of multislice computed tomography coronary angiography, Eur. Radiol. 17 (2007) 1842–1849.
[31] Stephan Achenbach, et al., Influence of slice thickness and reconstruction kernel on the computed tomographic attenuation of coronary atherosclerotic plaque, Journal of cardiovascular computed tomography 4 (2) (2010) 110–115.
[32] Suhny Abbara, et al., SCCT guidelines for the performance and acquisition of coronary computed tomographic angiography: a report of the society of cardiovascular computed tomography guidelines committee: endorsed by the north American society for cardiovascular imaging, Journal of cardiovascular computed tomography 10 (6) (2016) 435–449.
[33] Lucas L. Geyer, et al., State of the art: iterative CT reconstruction techniques, Radiology 276 (2) (2015) 339–357.
[34] Jr Dodge, J. Theodore, et al., Lumen diameter of normal human coronary arteries. Influence of age, sex, anatomic variation, and left ventricular hypertrophy or dilation, Circulation 86 (1) (1992) 232–246.